Numerical Modelling of Induced Seismicity along a Fault during CO_2 Injection into a Subsurface Reservoir

James E. J. Burtonshaw
Imperial College of Science, Technology and Medicine, London, United Kingdom

Adriana Paluszny
Imperial College of Science, Technology and Medicine, London, United Kingdom

Robert W. Zimmerman
Imperial College of Science, Technology and Medicine, London, United Kingdom

ABSTRACT: Injection, storage, and production of fluids in geological media could be a pivotal technology in the energy transition. Injection of fluid into subsurface systems is known to have the potential to induce seismic activity. The present work models induced seismicity during CO_2 injection using a three-dimensional finite element-based numerical simulator, the Imperial College Geomechanics Toolkit. Simulations quantify fault slip along a single fault in a five-layer domain of varying permeability. Fluid injection occurs at the left boundary over a period of hundreds to thousands of days, and induced seismicity is monitored during the injection period. Results for varying mesh refinement and properties are compared against a published scenario. The originally two-dimensional model is replicated in 3D, and the same set of material properties are considered, with permeabilities ranging from 10^{-14} to 10^{-19} m^2. The simulations predict peak slip to within a few centimeters of that of the numerical comparison study.

Keywords: Underground Fluid Storage, CCS, Induced Seismicity, Fault Slip, Meshing.

1 INTRODUCTION

The storage of gaseous fluids in porous subsurface systems such as depleted oil and gas reservoirs and aquifers is a promising method of storing renewable energy at the GigaWatt to TerraWatt scale. Geomechanical phenomena such as induced seismicity along pre-existing faults, micro-seismicity along new fractures, caprock fracturing, and surface subsidence may potentially all result from either the injection, production, or long-term storage of these fluids. Induced seismicity is important to study because geo-energy storage activities require a social license to operate from the public, and fault reactivation could displace units in a structural trap or rupture the caprock leading to seal loss and ultimately loss of the stored fluid.

To ensure a numerical simulator can accurately reproduce geomechanical behavior during the injection of gaseous fluids, its predictions should be validated against multiple analytical, semi-analytical and numerical solutions. In this paper, the results of simulations with the ICGT numerical simulator are compared with a previous numerical study (Mortezaei & Vahedifard, 2015) of fault

slip during carbon dioxide injection into a subsurface geological reservoir, that was conducted with the COMSOL simulator.

2 METHODOLOGY AND BACKGROUND

A 3-D, finite element method (FEM), fully-coupled, linear elastic fracture mechanics-based, hydromechanical simulator, the Imperial College Geomechanics Toolkit (ICGT), coded in C++ and applied in the fields of numerical simulation, CO_2 storage, fracture networks and fracture growth, borehole stability, charge blasting among others, is implemented for this work. The ICGT makes use of the Fraunhofer SAMG solver for inversion of the FEM matrix, and the ANSYS ICEM octree mesher to discretize the geometry. Friction is handled using an Augmented Lagrangian approach, with two outer and two inner Uzawa iterations (Nejati *et al.*, 2016), with fully-coupled iterative solution of displacement and fluid pressure. A detailed explanation of the computational nature of the ICGT, and the physics implemented, can be found in several publications (Paluszny & Zimmerman, 2011; Thomas *et al*., 2017; Salimzadeh *et al*., 2018).

Mortezaei & Vahedifard (2015) constructed a two-dimensional FEM thermo-hydro-mechanical model of a subsurface layer cake system consisting of five layers: an upper aquifer, an upper caprock, a reservoir, a lower caprock, and a lower aquifer unit. The model contains one fault that penetrates to some extent all five structural units (Figure 1). They performed a parametric study, varying the permeability and porosity of the reservoir units, and subsequently assessing the change in the slip along the fault. The prediction of fault slip was given at different times after the inception of injection depending on the permeability/porosity. The model has a square geometry with dimensions of 2000 × 2000 m. The fault is 1000 m long and is oriented at 80 degrees to the horizontal. The geometry is meshed with triangles, and the region around the fault is locally refined beyond the 'medium' mesh size of the model. The reservoir and caprock units were meshed with typically only two to four elements in the vertical direction, except where locally refined in the immediate vicinity of the fault. The upper and lower aquifer units were discretized with thirteen to fourteen elements in the vertical direction. CO_2 was injected as a point source at a rate of 0.02 kg/s at a depth of 1500 m at the center depth of the reservoir unit on the left boundary of the model. The material properties used for each structural unit are provided in Table 1m and these are replicated in the present model. The matrix pressure is constrained at the top and bottom to be 5 MPa and 24.63 MPa, respectively. The matrix temperature is constrained at the top and bottom to be 22.5 ºC and 72.5 ºC, respectively. Mechanical boundary conditions are a fixed bottom boundary, and vertical boundaries that can only move in the vertical plane, whereas the flow boundary conditions are set to be no flow through any boundary. Modelling was performed in the commercial multi-physics solver 'COMSOL Multiphysics'.

Table 1. Material properties of the five structural units within the model. Nomenclature: E = Young's Modulus, ν = Poisson's Ratio, ρ_s = Solid Density, α = Biot Coefficient, K = Permeability.

Structural Unit	E (GPa)	ν	ρ_s (kg/m^3)	α	K (m^2)
Upper Aquifer	10	0.25	1,280	1	1×10^{-14}
Upper Caprock	10	0.25	1,280	1	1×10^{-19}
Reservoir	10	0.25	1,280	1	Varied
Lower Caprock	10	0.25	1,280	1	1×10^{-19}
Lower Aquifer	10	0.25	1,280	1	1×10^{-16}

In the present work, the model is extended to three dimensions, and is cuboidal with dimensions of 2000 × 750 × 2000 m. The fault is extended from a line to a rectangle with a width equal to the length of the model in the y-direction (750 m). The initial study was thermo-hydro-mechanical, whereas this study is hydromechanical. To account for the variation in fluid properties with varying temperature in the original study, the fluid properties are varied slightly at the beginning of the simulations depending on depth within the model.

Table 2. Fluid properties of the fluids within each of the five structural units within the model. Nomenclature: μ = Viscosity, ρ_f = Fluid Density, B = Fluid Compressibility.

Structural Unit	Fluid	μ (Pa s)	ρ_f (kg/m^3)	B (Pa^{-1})
Upper Aquifer	Brine	8.3365×10^{-4}	1,070	4.47×10^{-10}
Upper Caprock	Brine	6.628×10^{-4}	1,065	4.34×10^{-10}
Reservoir	CO_2	7.5×10^{-5}	850	1.3×10^{-8}
Lower Caprock	Brine	6.103×10^{-4}	1,065	4.26×10^{-10}
Lower Aquifer	Brine	5.0785×10^{-4}	1,060	4.24×10^{-10}

For example, the brine in the upper caprock has different properties to the brine in the lower caprock (Table 2) which reflects the initial pressure and temperature of the mid-depth of each unit according to various P-T fluid property studies. The wellbore is modelled as a line element along the length of the left boundary of the domain.

3 RESULTS AND DISCUSSION

This section reports and discusses the results of four sets of numerical experiments: a comparison of (1) the effects of different fault mesh refinement on the pressure field and slip distribution; (2) the effects of different bulk rock mesh refinements on the pressure field and slip distributions; (3) the ICGT's prediction of fault slip for three different reservoir permeability cases of 1×10^{-12}, 1×10^{-13} and 1×10^{-14} m^2 against those of Mortezaei & Vahedifard (2015); and (4) the same as in (3) but for three different reservoir porosities of 0.10, 0.15, and 0.20. It must be noted that the numerical solution of Mortezaei & Vahedifard (2015) is not compared against any other data or simulations, and as such does not necessarily provide a true validation of the present simulations.

Firstly, four simulations with different bulk rock mesh refinements (Figure 1a) were performed, using isoparametric quadratic triangle and tetrahedral elements, to observe the effect of refinement on the fault slip distribution. The number of nodes per simulation varied between approximately 40k and 1,400k, whilst the number of elements varied between 30k and 1,000k.

The ICGT's prediction of the fault slip distribution is plotted in Figure 3, and shows a weak dependency on the bulk rock mesh refinement, varying by a maximum of 7-8 cm between different mesh refinements. This degree of variance is only observed near the peak slip within the reservoir and upper caprock units, with typically only 2-3 cm variation at the majority of depths along the fault. The fault slip solution converges once the mesh contains > 900k nodes, with the two highest refinement cases producing almost identical results. It is concluded that a coarser mesh overpredicts the slip, since the peak slip decreases as the number of nodes and elements increases.

Figure 2a displays the matrix pressure for each of the four refinement cases. The pressure is unstable in the coarsest case (approximately 40k nodes), especially along the bottom boundary of the domain and along the top of the upper caprock-upper aquifer interface. These zones typically correspond to the regions with the largest elements (Figure 1a). The stability of the solution drastically increases as the number of nodes increases to approximately 140k; however, some instability still arises particularly along the bottom boundary. The solution becomes completely stable in the case with approximately 910k nodes with a smooth gradient in pressure everywhere. Furthermore, the pressure in the left portion of the reservoir interval, corresponding to the injectant plume, converges with over 910k nodes. Therefore, it is important that the reservoir unit is particularly refined to ensure that the plume pressure is not a function of the mesh refinement. The remaining simulations in this work will use the mesh with approximately 910k nodes (Figure 1a).

Secondly, three simulations with the same bulk rock mesh refinement, but with different fault mesh refinements, were performed, and the effect of the fault refinement on the fault slip was examined. Figure 1b presents the three cases, varying from approximately 990 to 5.4k elements.

The ICGT's prediction of the fault slip distribution is shown in Figure 3, and shows that the fault slip is essentially insensitive to the fault refinement, at least within the range tested. Therefore, provided that at least approximately 1,000 elements discretize the fault mesh, the solution will be

accurate. The matrix pressure solution for the three cases is displayed in Figure 2b. The pressure solution converges with at least approximately 1,400 elements. In the coarsest case, where the fault is discretized with less than 1,000 elements, the pressure in the left portion of the reservoir is approximately 1 MPa less than that observed with higher fault refinements. This occurs because the coincident bulk rock mesh is coarser when the fault discretization is coarser, since the bulk rock mesh elements here are constrained by the size of the elements on the fault surfaces. All cases predict near-identical fault slip, but since the pressure field differs for the coarsest mesh, the remaining simulations in this work will use the fault mesh with approximately 1,400 elements (Figure 1b).

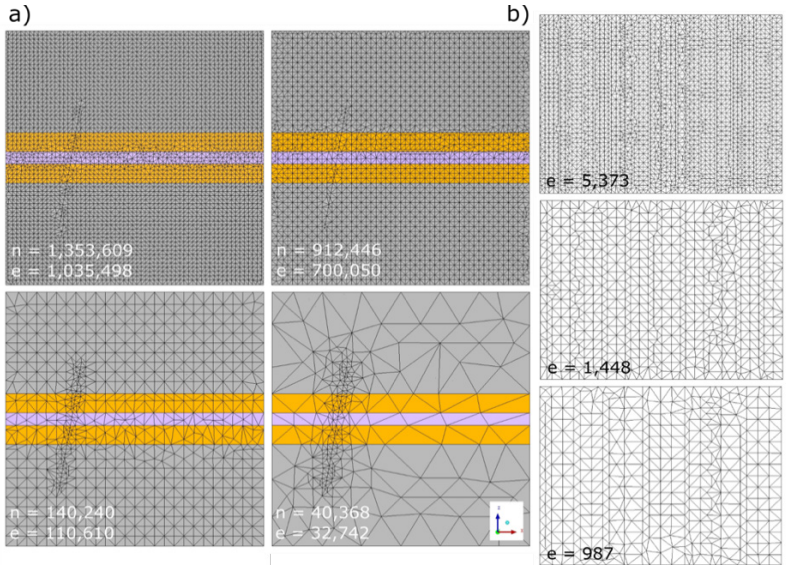

Figure 1. (a) Model mesh discretization for different bulk rock mesh refinements (view of the *x*-*z* cut-plane through center of domain). (b) Fault mesh discretization for different fault mesh refinements. Number of nodes is denoted by *n* and elements by *e*.

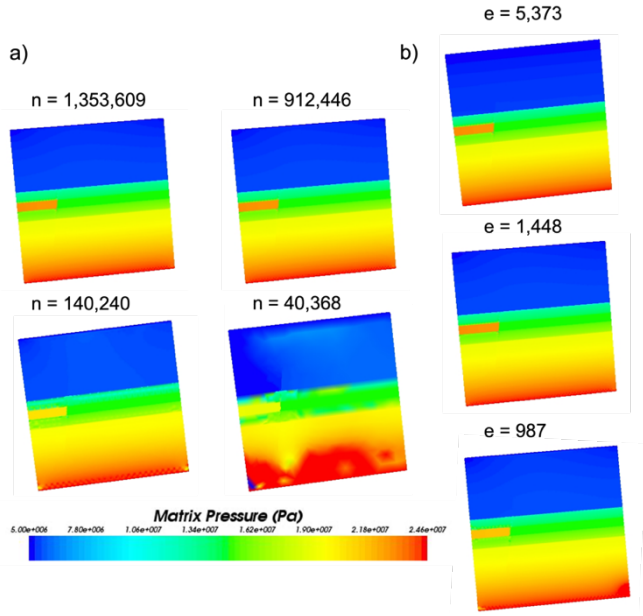

Figure 2. Matrix pressure across *x*-*z* cut-plane at the center of the domain for the 1×10^{-13} m^2 reservoir permeability case after a time of approximately 280 days. (a) bulk rock mesh refinement cases and (b) fault mesh refinement cases.

Thirdly, the results of three simulations in which the permeability of the reservoir unit was varied between 1×10^{-12} m^2 and 1×10^{-14} m^2 and fourthly, three simulations in which the porosity of the reservoir unit was varied between 0.10 and 0.20, as in the work of Mortezaei & Vahedifard (2015),

are presented. The bulk rock mesh used was that with approximately 900k elements in Figure 1a and the fault mesh used was that with approximately 1,400 elements in Figure 1b.

In the permeability cases, the ICGT's prediction of fault slip is presented in Figure 4. In each case, the peak fault slip is accurate relative to the numerical comparison. The 1×10^{-14} m^2 case was to within 5 cm, the 1×10^{-13} m^2 case to within 1 cm, and the 1×10^{-12} m^2 case to within 3 cm. The fault slip distribution as a function of depth is more gradual than the numerical comparison, where the slip is highly concentrated at the reservoir-upper caprock interface, and abruptly declines elsewhere.

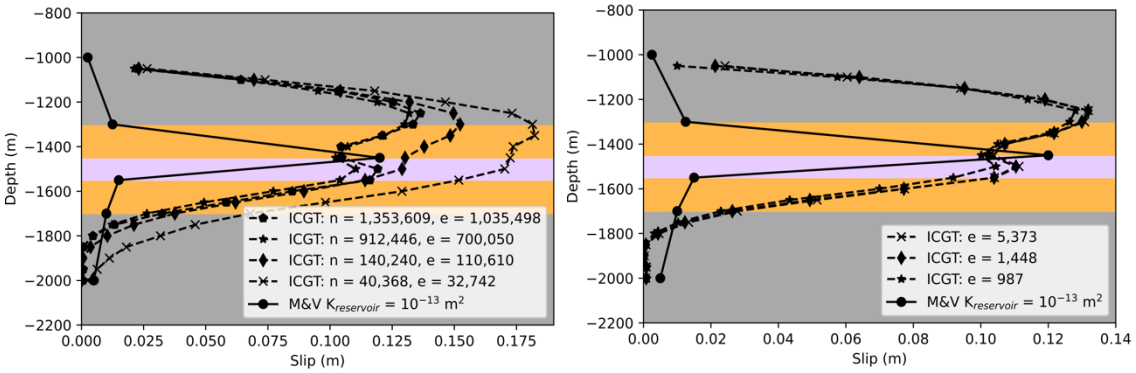

Figure 3. Model depth versus slip along the fault for (left) different rock matrix mesh and (right) fault mesh refinements for the 1×10^{-13} m^2 reservoir permeability case after a time of approximately 280 days. The number of elements and nodes are denoted by e and n, respectively. The dashed lines represent results generated from the ICGT.

The matrix pressure solution is shown in Figure 5 for each of the permeability cases. The pressure in the left portion of the reservoir increases from left to right. This reflects both the decreasing reservoir permeability from left to right, but also the increased injection time since the 10^{-12} m^2, 10^{-13} m^2, and 10^{-14} m^2 cases display the matrix pressure after approximately 110, 280, and 1400 days, respectively. In the 10^{-14} m^2 permeability case, the far larger injection time has allowed the plume pressure to have significantly diffused into the upper and lower caprock units and into the lower aquifer unit, which is likely responsible for the larger slip (relative to the higher permeability cases) at most fault depths away from the peak slip predicted by Mortezaei & Vahedifard (2015) and observed, but less so, in the ICGT predictions (Figure 4).

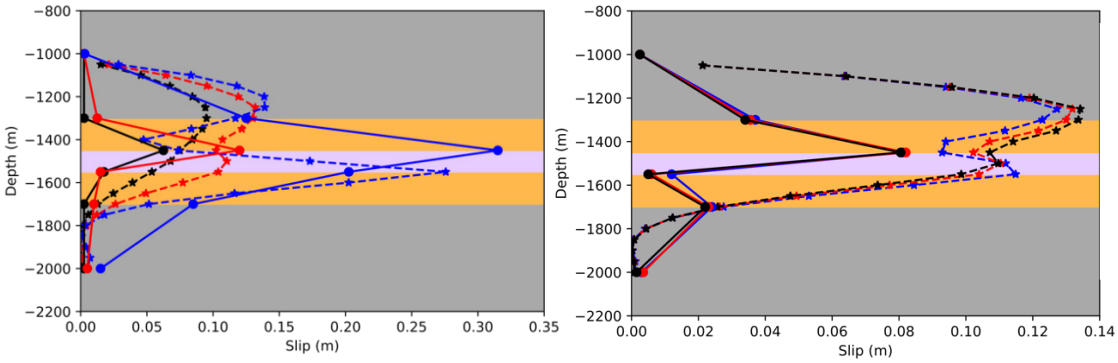

Figure 4. Model depth versus slip along the fault for (left) different permeability and (right) porosity cases after injections times of approximately 110, 280, 1400 days and 270, 310, 340 days in the 10^{-12} (blue), 10^{-13} (red), 10^{-14} m^2 (black) permeability and 0.10 (blue), 0.15 (red), and 0.20 (black) porosity cases, respectively. The dashed lines represent results generated from the ICGT. The solid lines represents the results of Mortezaei & Vahedifard (2015).

In the cases in which porosity was varied, the ICGT's prediction of fault slip is shown in Figure 4. The peak fault slip is slightly overpredicted by 1.5 cm, 2 cm, and 2.5 cm in the 0.10, 0.15, and 0.20 porosity cases, respectively. However, in each of these cases, the absolute error is small. The ICGT effectively replicates the general trend that the fault slip is relatively insensitive to reservoir porosity.

This is shown by the lines representative of the ICGT results plotting on top of each other at all depths, except some within the upper caprock and reservoir units where there is only a maximum of 1 cm of difference in slip.

Figure 5 presents the matrix pressure field in each of the porosity cases. As expected, the matrix pressure is essentially identical in all three cases, which supports the insensitivity of fault slip to the porosity, as seen in Figure 4. Simulations were also performed for isoparametric linear triangle and tetrahedral elements, and for isoparametric linear quadrilateral and hexahedral elements. These yielded comparative results with variations within the 5 cm range.

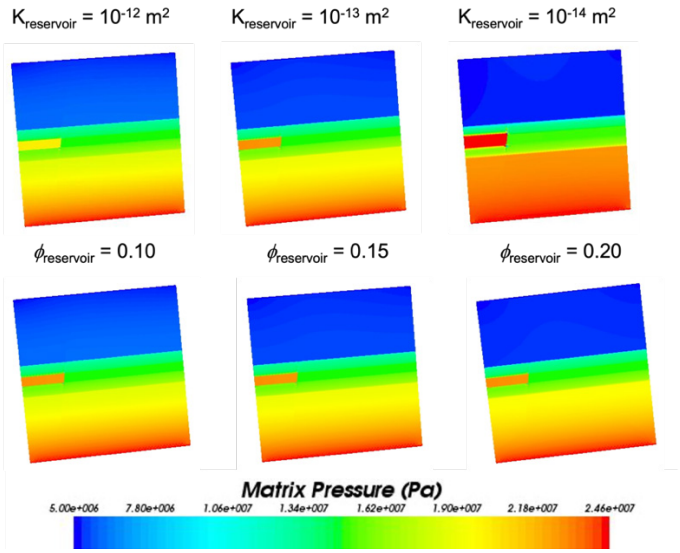

Figure 5. Matrix pressure across *x-z* cut-plane at the center of the domain for different permeability and porosity cases after injection times of approximately 110, 280, 1400 days and 270, 310, 340 days.

4 CONCLUSION

A comparative study of slip modelling along a single fault was performed for injection of carbon dioxide into a subsurface reservoir. Following the selection of suitable fault and bulk rock meshes, the prediction of the ICGT was compared against the numerical solution of Mortezaei & Vahedifard (2015) for three cases of varying reservoir permeabilities, and three cases of varying reservoir porosities. The ICGT reservoir permeability cases successfully predicted the peak fault slip to within 1–5 cm. The ICGT reservoir porosity cases displayed the same behavior as in the numerical comparison, and the peak slip variation was approximately within 5 cm in all cases. The ICGT has been shown to be capable of replicating injection-induced fault slip prediction results to within a reasonable precision. The observed small-scale over-predictions in fault slip can be probably be attributed to the lack of thermal conduction and dynamic property variation modelling, which will be part of future work.

REFERENCES

Mortezaei, K. and Vahedifard, F. 2015. Numerical simulation of induced seismicity in carbon capture and storage projects. *Geotechnical and Geological Engineering*, 33(2), pp. 411-424.

Nejati, M., Paluszny, A. and Zimmerman, R.W. 2016. A finite element framework for modeling internal frictional contact in three-dimensional fractured media using unstructured tetrahedral meshes. *Computer Methods in Applied Mechanics and Engineering*, *306*, pp. 123-150.

Paluszny, A. and Zimmerman, R.W. 2011. Numerical simulation of multiple 3D fracture propagation using arbitrary meshes. *Computer Methods in Applied Mechanics and Engineering*, 200(9-12), pp. 953-966.

Salimzadeh, S., Paluszny, A., Nick, H.M. and Zimmerman, R.W. 2018. A three-dimensional coupled thermo-hydro-mechanical model for deformable fractured geothermal systems. *Geothermics*, 71, pp. 212-224.

Thomas, R.N., Paluszny, A. and Zimmerman, R.W. 2017. Quantification of fracture interaction using stress intensity factor variation maps. *Journal of Geophysical Research: Solid Earth*, 122(10), pp. 7698-7717.